JSR Publications

Available Online

J. Sci. Res. **9** (4), 383-402 (2017)

JOURNAL OF SCIENTIFIC RESEARCH

www.banglajol.info/index.php/JSR

Copper-doped Hydroxyapatite for Removal of Arsenic(V) from Aqueous System

S. A. Jahan[1], M. Y. A. Mollah[2], S. Ahmed[1], M. A. B. H. Susan[3]*

[1]Bangladesh Council of Scientific and Industrial Research (BCSIR), Dr. Qudrat-I-Khuda Road, Dhaka-1205, Bangladesh

[2]University Grants Commission of Bangladesh, 29/1 Agargaon, Sher-E-Bangla Nagar, Dhaka-1207, Bangladesh

[3]Department of Chemistry, University of Dhaka, Dhaka-1000, Bangladesh

Received 16 May 2017, accepted in final revised form 10 September 2017

Abstract

In this work, pure and copper-doped hydroxyapatite (various wt% of Cu) were synthesized by wet chemical precipitation method using eggshells as source of calcium. The efficiency of the prepared materials for removal of arsenic(V) from aqueous system has been investigated. Pure and Cu(II)-doped HAP were calcined at different temperatures ranging from 100-600 °C. The synthesized HAPs were characterized by Fourier Transform Infrared (FT-IR) spectroscopy, X-ray Diffraction (XRD), Scanning Electron Microscopy (SEM), Energy Dispersive X-ray Spectroscpic Analysis (EDS), particle size analysis based on dynamic light scattering measurements, and Brunauer–Emmett–Teller (BET) surface area analysis. FT-IR spectra and XRD patterns of synthesized HAPs confirmed the formation of single HAP phase. XRD patterns showed decrease in crystallite size for Cu-HAP compared to pristine HAP. BET surface area of Cu-HAP calcined at 300 °C increased to 153.39 m^2g^{-1} from 66.80 m^2g^{-1} for pure HAP. Finally, the synthesized HAPs were applied to remove As(V) from aqueous system. As(V) removal efficiency for Cu-HAP was two-fold higher than that of pure HAP. Adsorption behaviors were analyzed for As(V) adsorption on thermally treated pure and Cu-HAP using Langmuir, Freundlich, and Temkin adsorption isotherms. Finally, the prospect of Cu(II)-doped HAP for treatment of waste water containing heavy metals has been discussed.

Keywords: Hydroxyapatite; Arsenic; Surface area; Adsorption isotherm.

doi: http://dx.doi.org/10.3329/jsr.v9i4.32606 J. Sci. Res. **9** (4), 383-402 (2017)

1. Introduction

Arsenic, classified as a group 1 human carcinogenic substance by the World Health Organization (WHO) [1], has been reported in significant concentration in ground water

* *Corresponding author:* susan@du.ac.bd

in Bangladesh, Chile, China, India and few other countries [2]. Based on WHO guidelines, arsenic concentrations in drinking water should be strictly limited to 10 μgL^{-1} [3]. Chronic intake of inorganic arsenic as drinking water or else with concentrations above this limit, may cause arsenicosis [4]. Arsenic(V) is generally the most common arsenic species present in the well oxygenated surface water [5]. Anthropogenic activities like manufacture of paints, dyes, ceramics and glass, electronics, pigments, antifouling agents, and agricultural uses as pesticides, herbicides are reported to promote the presence of As(V) in the environment [6]. A survey reports that about 80 million people in Bangladesh are exposed to contaminated groundwater having concentrations above Bangladesh standard of 50 μgL^{-1} [7,8].

Considerable volume of work has been carried out to remove As(V) from contaminated water. Adsorption is considered to be superior to other traditional methods used for the removal of As(V) due to its low cost [9], relatively high arsenic removal efficiencies [10, 11], ease of operation and handling [12]. A wide variety of adsorbents have already been studied including activated carbon, fly ash, goethite, zeolites, activated alumina, titanium dioxide, iron hydroxide, zero-valent iron, and cation-exchange resins [13-15]. However, most of these adsorbents are either less effective to remove arsenic or too expensive for use as an adsorbent. It is, therefore, quite pertinent to develop new adsorbents which are cheap, more efficient, and rapid towards arsenic ingestion. Recently hydroxyapatite (HAP) attracts the attention of the researchers as a potential adsorbent for toxic heavy metals due to its large specific area, high thermal and chemical stability, and high ionic exchange capacity [16]. Synthesis of HAP from bio-waste (eggshell) will be a significant step to lower the synthetic cost. As Cu(II) have strong affinity for arsenate than Ca(II) [17], it is expected that incorporation of Cu(II) in HAP will increase the As(V) removal efficiency of the material.

The work aims at preparing pure and Cu(II)-doped HAPs from a bio-waste, eggshell and thermally treat to optimize the adsorption capacity for efficient removal of arsenic(V) from aqueous system.

2. Experimental

2.1. *Materials*

Analar grade chemicals di-ammonium hydrogen phosphate (BDH, England), sodium borohydride (Lancaster, England), potassium iodide (Merck, Germany) and copper nitrate (Merck, Germany) were used without further purification. All the substrate solutions were prepared using distilled de-ionized (DI) water with specific conductivity 1.70 μScm^{-1} at 29.5 °C. Eggshells were used as a calcium precursor to the synthesis of pure and Cu(II)-doped HAP.

2.2. *Synthesis of pure and Cu(II)-doped HAP using wet chemical method*

For the preparation of 0.95 M calcium precursor solution, 25 g of eggshell powder was dissolved in 50 mL of concentrated nitric acid. The mixture was filtered to obtain a clear solution and was transferred to a 250 mL volumetric flask and DI water was added up to the mark. 0.57 M phosphate precursor solution was prepared by dissolving 18.69 g of $(NH_4)_2HPO_4$ in a 250 mL volumetric flask with DI water. The phosphate precursor solution was slowly added to the calcium precursor solution with continuous stirring at room temperature (29 ± 1 °C) and the pH of the solution was adjusted to ca. 10 by using aqueous NH_3. The Ca/P ratio was maintained 1.67. A gelatinous precipitate was formed and the slurry was then kept for 24 h. The precipitate was then filtered and washed with water up to 10 times. Finally, the product was thermally treated at temperatures 110, 300 and 600 °C. The calcination temperatures were achieved raising the temperature at the rate of 3°Cmin^{-1} with 1 h soaking time. Cu(II)-doped HAP (Cu-HAP) was synthesized by adding Cu^{2+} ion solution to calcium precursor prior to the addition of phosphate precursor in the same process. Different quantity of doping salt was used in the synthesis of Cu-HAP. Fig.1. shows the schematic diagram of the synthesis of pure and Cu-HAP from eggshells. Table 1 summarizes the sample history.

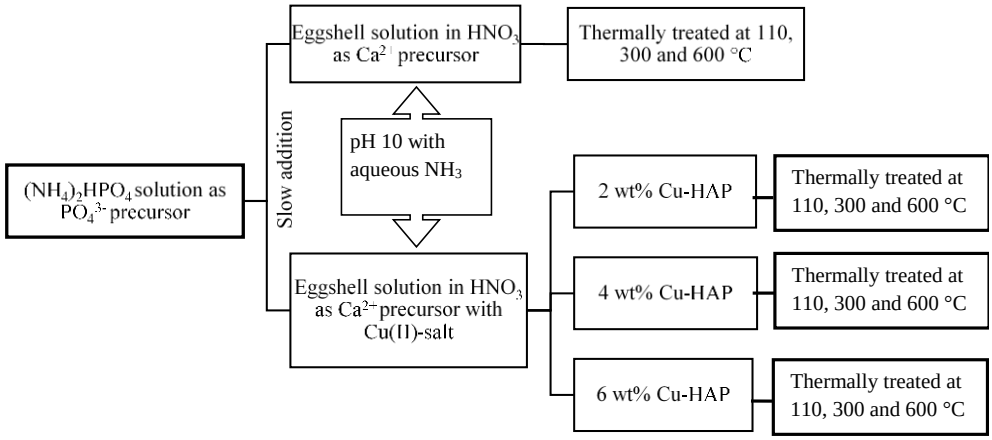

Fig. 1. Schematic diagram for synthesis of pure and Cu-HAP from eggshell.

2.3. *Characterization of pure and Cu-HAP*

Diffractograms of pure and Cu-HAP were recorded by an x-ray diffractometer (PANalytical X'Pert PRO PW 3040) using CuK_α (λ= 1.5418 Å) radiation generated at 40 kV and 30 mA within the scan range 2θ = 5 to 75° with a step size (2θ) of 0.02°. The phases formed were validated by comparing with the respective standard of Joint Committee on Powder Diffraction (JCPDS) files.

The infrared spectra were recorded in the wavenumber range from 4000 to 400 cm^{-1} with 4 cm^{-1} resolution using a Fourier transform infrared (FT-IR) spectrophotometer

(Prestige21 Shimadzu). A powdered sample (approximately 1 mg) was mixed with about 100 mg of anhydrous KBr to prepare the pellet.

Table 1. Sample code of pure and Cu-HAP.

Sample	Wt % $Cu(NO_3)_2$	Calcination temperature (°C)	Sample code
Pure HAP	0.0	110	HAP1
		300	HAP3
		600	HAP6
2%Cu-HAP	2.0	110	2%Cu-HAP1
		300	2%Cu-HAP3
		600	2%Cu-HAP6
4%Cu-HAP	4.0	110	4%Cu-HAP1
		300	4%Cu-HAP3
		600	4%Cu-HAP6
6%Cu-HAP	6.0	110	6%Cu-HAP1
		300	6%Cu-HAP3
		600	6%Cu-HAP6

Morphological characterization of the samples was carried out by scanning electron microscopy (SEM) using a Hitachi S-3400 N equipped with energy dispersive spectrophotometer (EDS).

Particle size was measured by dynamic light scattering (DLS) technique using Zetasizer Nano ZS90 (ZEN3690, Malvern Instruments Ltd). A He–Ne laser beam of 632.8 nm wavelength was used as light source and the measurements were made at a fixed scattering angle of 90°. The scattering intensity data were analyzed to obtain the hydrodynamic diameter (D_h). Using a cell of 10 mm diameter, a specific amount of HAP powder was subjected to ultrasonic treatment in aqueous medium for 20 min which facilitated minimum degree of agglomeration. The particle sizes were determined from the translational diffusion coefficient using the Stokes–Einstein equation [18].

In order to determine surface area, pure and Cu-HAP were pretreated by purging N_2 gas for 4 h adjusting heating temperature at 120 °C to remove moisture and organic impurities from the surface of the particles. Pretreatment of the samples were performed by BELPREP-flowII (BEL Japan, Inc.) and the measurements were carried out by BEL sorp mini II (BEL Japan, Inc.). The adsorption isotherms, generated from N_2 gas adsorption-desorption data were used to analyze the pore size distribution, surface area, pore volume, and other properties. The isotherms have different shapes which depend on pore structure of solid as well as interaction between sample surface and adsorbate gas. IUPAC classifications were used to define both adsorption isotherms and adsorption hysteresis loops [19]. Surface area and pore size distribution of adsorbents were calculated from Brunauer, Emmett, and Teller (BET) isotherm [20] and Barrett, Joyner, and Halenda (BJH) plot [21] respectively which were prepared from the data of gas-adsorption measurements.

Hydride generation atomic absorption spectrophotometer (HG-AAS, NOVAA 350, Analytik Jena, Germany) was used to determine concentration of As(V) in aqueous

solution. AAS equipped with hydride generation and hollow cathode lamp operated at 10 mA was used for determination of arsenic(V). A spectral band width of 0.5 nm was selected to isolate the 193.7 nm arsenic(As) line. Calibration standards (2, 5, 10 and 20 μgL^{-1}) were prepared from the As(V) stock solution by appropriate dilution of the standard solutions and regression coefficient value (R^2) was >0.999. As(V) standards solution was prepared according to the standard procedure (SOP) reported by HG-AAS, NOVAA 350, Analytik Jena, Germany.

2.4. *Removal of arsenic from aqueous system using pure and Cu-HAP*

Batch experiments were conducted in well capped 150 mL flasks, containing 50 mL As(V) solution with the required concentrations. After the addition of specific amount of adsorbent, the flask was shaken in a thermostatic shaker at 150 rpm and 30 ºC for 60 min. The contents were then centrifuged at 2000 rpm for 15 min and the supernatant liquid was analyzed for As(V) ion concentration using hydride generated atomic absorption spectrophotometer (HG-AAS). The effect of pH in the range of 3.0 to 10.0 was studied with initial arsenic concentration 100 μgL^{-1}. The effect of adsorbent dosage was studied by varying the adsorbent dosage from 1 to 10 gL^{-1} at pH 9.0. The initial concentrations of the As(V) solutions were set from 65 to 170 μgL^{-1}. The adsorption isotherms were studied at 30 °C, pH 9.0 for As(V) and were fitted to Langmuir, Freundlich, and Temkin isotherm adsorption models. Samples were collected at different intervals in 100 μgL^{-1} of arsenic solution for kinetic study. The pH values of all the solutions were adjusted by adding HCl or NaOH solutions of desired concentrations.

The adsorption capacity of As(V) adsorbed per gram of adsorbent (μgg^{-1}) and percent of adsorption efficiency were calculated following equations. 1 and 2 [22], respectively.

$$q_e = \frac{V}{M} \times (C_i - C_f) \quad (1)$$

$$\text{Adsorption efficiency, \%} = \frac{(C_i - C_f)}{C_i} \times 100 \quad (2)$$

where C_i and C_f are the initial and final concentrations of the As(V) in the aqueous solution in μgL^{-1}, V is the volume of the adsorbate solution in L and M is the mass of the adsorbents in g used.

3. Results and Discussion

3.1. *Characterization of pure and Cu-HAP*

3.1.1. *Phase identification by XRD*

Fig. 2 shows the XRD patterns of oven dried pure and Cu-HAP as an example. Presence of strong diffraction peaks corresponding to HAP phase at 2θ position ~31.84° for (211)

reflection plane and two peaks at 32.18 and 32.89° confirms the formation of HAP phase in the samples [23]. XRD data are in good agreement with JCPDS file 09-0432 which correspond to hexagonal HAP. No significant change in peak positions is observed (Fig. 2), except the decrease in the intensity of peak for (002) plane with increase of Cu content in HAP structure. This is the indication of increase in amorphous nature of Cu-HAP with increase in Cu content in the samples. Ionic radius of Cu(II) (0.77 Å) is smaller than that of Ca(II) (0.99 Å) which induces strain on HAP crystal lattice, thus the crystallinity of the sample is decreased [24].

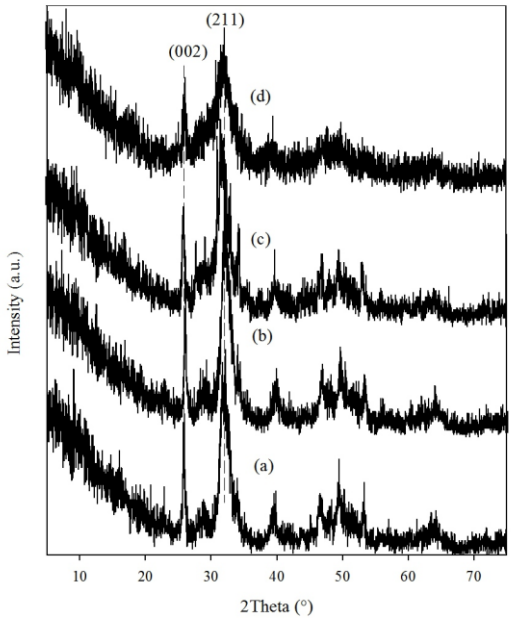

Fig. 2. XRD patterns of synthesized HAP calcined at 110 °C containing (a) 0, (b) 2, (c) 4 and (d) 6 wt% Cu.

XRD pattern of 2%Cu-HAP6 in Fig. 3 indicates the presence of a second phase along with HAP phase in the sample. XRD pattern shows major peak at 31.27° in 2θ for (210) reflection plane along with peak at 2θ position 34.68 for (220) plane which is almost in equal intensity of the major peak. This pattern is in agreement with JCPDS File 09 -0169 for *β-TCP* [25].

Effect of Cu(II) incorporation in HAP structure was studied by analyzing the crystallographic data. To ensure the formation of desired HAP together with β-TCP phase, crystallographic information was extensively verified. Crystallite size, lattice parameters (*a*, *c*) of HAP and β-TCP phases were calculated according to the procedures reported by Rezakhani *et al*. [26] and Kannan *et al.* [27] and parameters of the samples calcined at 600 °C are presented in Table 2 as an example.

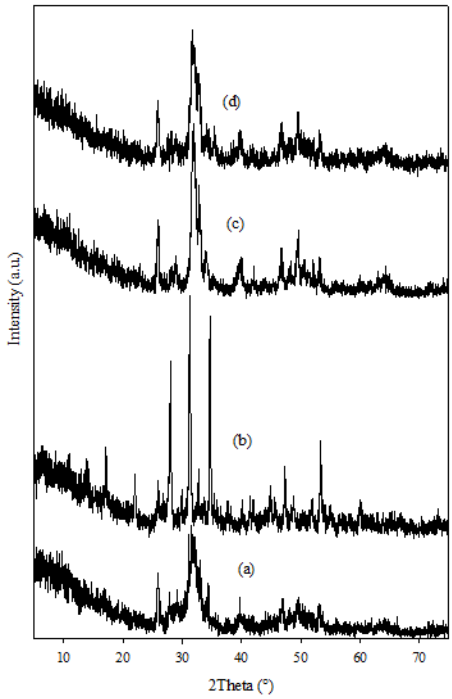

Fig. 3. XRD patterns of synthesized HAP calcined at 600 °C containing (a) 0, (b) 2, (c) 4, and (d) 6 wt% Cu.

Table 2. Calculated and JCPDS crystallographic parameters of Cu-HAP6.

Sample code	Phase and symmetry	Lattice constants (Å)		Crystallite size (nm)
		a = *b*	*c*	
2%Cu-HAP6	β-TCP Rhombohedral	10.35	37.49	78.83
4%Cu-HAP6	HAP Hexagonal	9.43	6.88	20.35
6%Cu-HAP6	HAP Hexagonal	9.44	6.88	23.07
JCPDS File # 09-0432	HAP Hexagonal	9.42	6.88	
JCPDS File # 09-0169	β-TCP Rhombohedral	10.43	37.38	

Lattice parameter *c* (Table 2) is in good agreement with the standard JCPDS value for all Cu-HAP6, while *a* value is slightly higher than that of standard value. This discrepancy could be due to the amorphous nature of Cu-HAP. Substitution of larger Ca^{2+} ion with relatively smaller Cu^{2+} ion is likely to exert strains in the HAP lattice, which affects the crystallite size at higher Cu content in Cu-HAP. It is reported that larger ions prefer to substitute Ca in the Ca-II site for HAP and provokes an increment in lattice parameter *a* but reduces lattice parameter *c* [28,29]. However, increase in the cell parameter *a* with no

change in the cell parameter *c* of 4% and 6%Cu-HAP6 indicates substitution at Ca-II site of the samples.

3.1.2. *Functional group analysis by FT-IR*

Presence of characteristic phosphate and hydroxyl groups in Cu-HAP were identified through FT-IR analyses. FT-IR spectra of Cu-HAP6 with different weight percent of Cu(II) are shown in Fig. 4. The bands at 1090-1030 cm^{-1} are due to the ν_3 stretching of PO_4^{3-} group, doublet at approximately 601–606 cm^{-1} and 560–566 cm^{-1} are due to the ν_4 bending mode of PO_4^{3-} group and very weak bands located at 956–962 cm^{-1} are attributed to ν_1 stretching mode of PO_4^{3-} present in Cu-HAP [30]. The peak at 1627 cm^{-1} and broad band at approximately 3440 cm^{-1} correspond to the water adsorbed on the surface of samples. The weak peak at approximately 3537 cm^{-1} can be ascribed to the stretching vibration mode of the structural OH^- group in the lattice. Band appearing at ~2360 cm^{-1} corresponds to the presence of CO_3^{2-} incorporated from the atmospheric CO_2 which was introduced during the wet chemical synthesis of HAP [31]. Incorporation of CO_3^{2-} ions suggests substitution of phosphate in the apatite lattice. Absorption peaks at 870, 1319, 1419, and 1457 cm^{-1} indicate β-type substitution of carbonate group in HAP [32, 33]. Stretching vibration for structural OH group has mostly been masked by the broad H_2O absorption band and is observed as a shoulder at 3570 cm^{-1} [34].

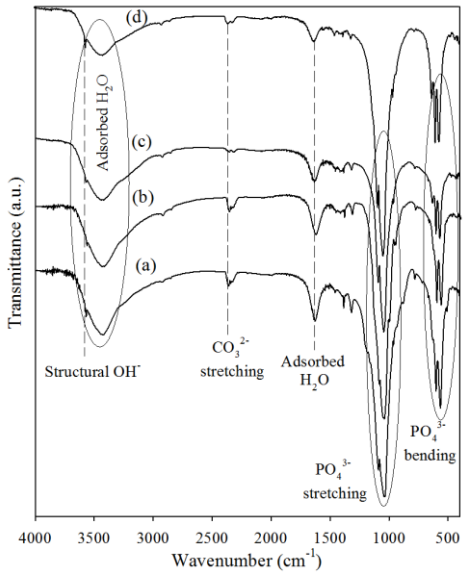

Fig. 4. FT-IR spectra of Cu-HAP from eggshell containing (a) 0, (b) 2, (c) 4 and (d) 6 wt% Cu.

However characteristic vibration bands for phosphate group in HAP structure remain unchanged in Cu-HAP. This can be attributed to the fact that thermal treatment of Cu-HAP does not make any change to the HAP phase in the samples.

3.1.3. *Morphology analysis by SEM*

Fig. 5 shows SEM images of HAP6 with and without Cu(II). Agglomeration of Cu-HAP is noticeable at high concentrations of Cu(II) in particular at high calcination temperatures. This can be attributed to the fact that increase in calciation temperature as well as the amount of dopant resulted in an amalgamation of the smaller particles of the sample. SEM images (Fig. 5b, 5c) indicate an agglomeration of the particles analyzed with an increase in Cu(II) content from 2wt% to 4wt%. On the other hand, homogenous distribution is observed in Fig. 5b for 2%Cu-HAP6. The particle size of 2%Cu-HAP6 was smaller as compared to pure HAP and 4%Cu-HAP6.

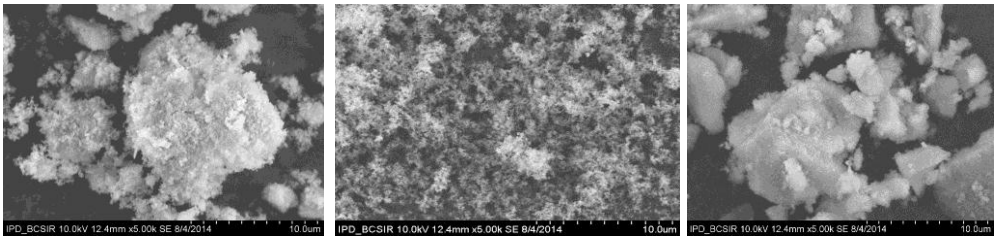

(a) (b) (c)

Fig. 5. SEM images of Cu-HAP6 containing (a) 0, (b) 2 and (c) 4 wt% Cu(II).

3.1.4. *Elemental analysis by EDS*

Chemical compositions of all the synthesized samples were determined by EDS analyses. Fig. 6 shows the presence of Cu along with Ca, P and O with a small amount of carbon in the Cu-HAP sample. The (Ca+Cu)/P ratio of the sample is calculated as 1.40 which is less than the expected value of 1.67 for bones. Synthesis of non-stoichiometric Cu-HAP may be attributed to the presence of small amount of carbon in the products.

3.1.5. *Analysis of nitrogen adsorption behavior*

Specific surface area and total pore volume were measured using N_2 gas (at 77K) adsorption/desorption isotherm. The isotherms for thermally treated Cu-HAP both oven dried and calcined at 300 °C are shown in Fig. 7. Adsorption–desorption isotherm for 2%Cu-HAP1 (Fig. 7(a)) illustrates type III isotherm with no hysteresis loop. This indicates adsorption on a non-porous surface and surface area of the sample is also very low. Type III isotherm with narrow H1 hysteresis loop for 2%Cu-HAP3 in Fig. 7(b) indicates the presence of a narrow distribution of relatively uniform cylindrical or tubular pores [35].

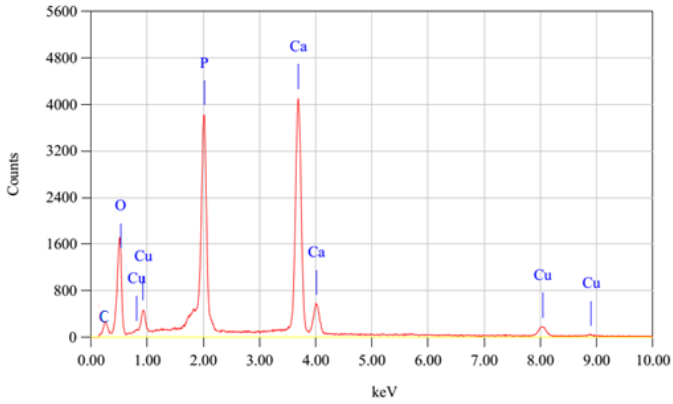

Fig. 6. EDS spectrum of Cu-HAP from eggshell.

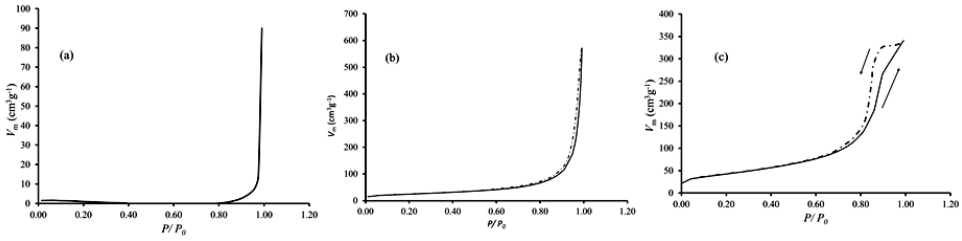

Fig. 7. Adsorption/ desorption isotherm of (a) 2%Cu-HAP1 (b) 2%Cu-HAP3 and (c) 6% Cu-HAP3.

3.1.6. *Analysis of adsorption data by BET isotherm*

Parameters obtained from the analyses of BET plot and BJH plot for Cu-HAP are given in Table 3. The lower specific surface area and the pore volumes of 2%Cu-HAP1 is possibly due to the blockage of internal pores by incorporation of Cu^{2+} ions. Since mean pore diameter of the oven dried sample is larger than calcined Cu-HAP sample, blocked pores are likely to be micropores, resulting in a decrease of specific surface area and total pore volume.

Table 3. Data obtained from analysis of BET isotherms and BJH plot for Cu-HAP.

Sample code	BET surface area, (m^2g^{-1})	BJH total pore volume, (cm^3g^{1})	BJH micropore diameter, (nm)
2%Cu-HAP1	6.50	0.1311	94.44
2%Cu-HAP3	86.44	0.8803	13.90
6%Cu-HAP3	153.39	0.5383	13.73

BJH plot (Fig. 8a) shows the pore size distribution which indicates the presence of macropores along with mesopores in the sample. Surface area of calcined Cu-HAP

increases with increasing concentration of dopant. However total pore volume decreases with decrease in crystallite size of the samples. Increase in amount of copper in Cu-HAP increases specific surface area which indicates incorporation of Cu^{2+} ions in Ca sites in HAP matrices. Effect of doping of Cu^{2+} ion is also consistent with particle size of the samples determined from BET measurements (Table 3).

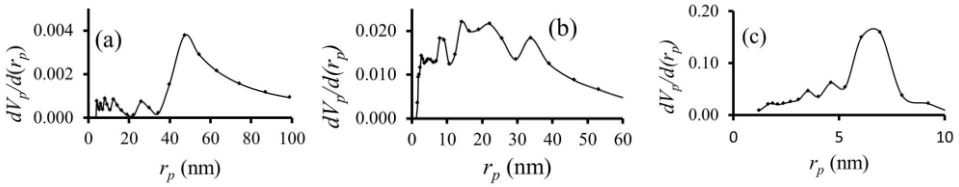

Fig. 8. Differential curves of BJH plot of a N_2 adsorption isotherm of (a) 2%Cu-HAP1, (b) 2%Cu-HAP3 and (c) 6%Cu-HAP3.

3.1.7. *Particle size and its distribution*

Dynamic light scattering technique was used to determine the particle size distribution (Fig. 9) and average particle size of Cu-HAP. DLS results show that the average particle size decreases from 2.67 µm to 0.47 µm when Cu(II) content increases in the samples from 2wt% to 6wt%. Pure HAP6 has the average particle size of 4.21 µm which is higher as compared to HAP doped with Cu(II). The DLS measurements show correlograms (correlation intensity vs. time; Fig. not shown) with indication of stable species in the system without any sedimentation and aggregation during the course of measurements. In fact, even after prolonged period, no sedimentation or aggregation could be marked.

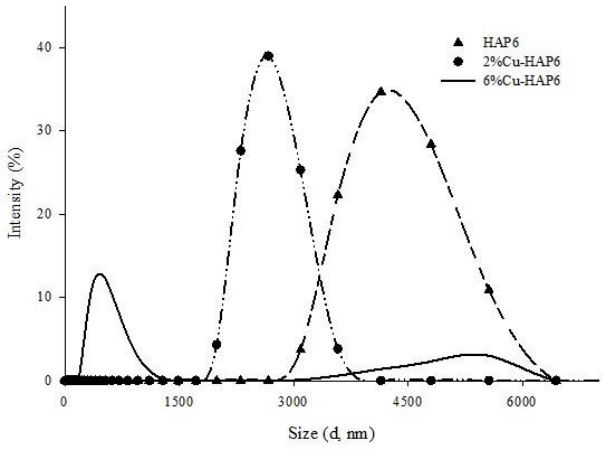

Fig. 9. Particle size distributions of Pure and Cu-HAP.

3.2. *Adsorption properties*

The optimization of the adsorption parameters was achieved by varying various experimental variables. The optimized adsorption parameters were concentration of arsenate, contact time, pH, and adsorbent dosage.

3.2.1. *Effect of contact time*

Fig. 10 shows the effect of contact time on the percentage removal of As(V) using pure and Cu-doped HAP at optimum pH at 30 °C. Initial As(V) concentration was 100 μgL^{-1}. Percentage of As(V) removal efficiency increase with increasing the contact time. Most of adsorption takes place in the initial 20-30 min and then increases slowly and reaches the maximum adsorption in about 50 to 60 min for all adsorbents. Fig. 10 shows that 15.5% adsorption occurs for thermally treated pure HAP in the first 30 min and reaches equilibrium at 60 min with slow increase in efficiency up to 22.5%. Nevertheless initial adsorption efficiency of Cu-HAP are in the range of 23-38% which finally reached at equilibrium with 33-49%. It is obvious from Fig. 10 that doping of pure HAP increases the adsorption capacity by approximately two fold for Cu(II) doped products. Rate of removal of As(V) is higher at the initial stage, due to the availability of more active sites on the surface of pure as well as Cu-HAP. The rate is slower at the later stages probably due to the electrostatic hindrances between negatively charged arsenate species adsorbed on the surface of adsorbents and also due to the reduction of active sites on adsorbents [36]. Slower adsorption rate may also be due to the slower rate of diffusion of arsenate Cu-HAP [37].

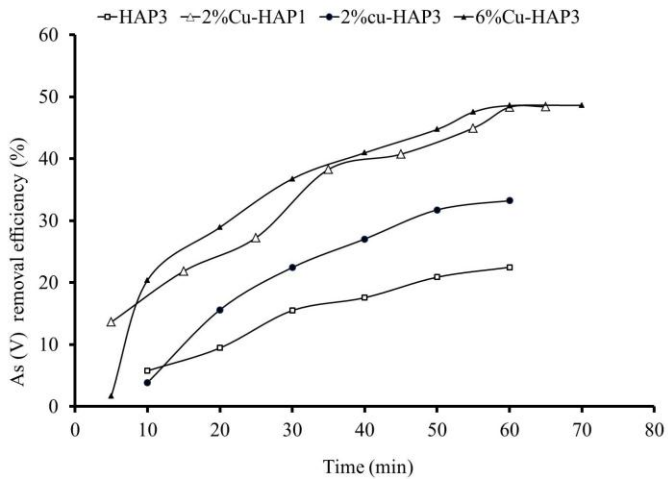

Fig. 10. Effect of contact time on removal of As(V) by pure and Cu-HAP.

3.2.2. *Effect of initial pH*

The pH of the medium influences adsorption and strongly controls the speciation of the arsenic in aqueous system [38]. The type of specific arsenic species available for adsorption is also dependent on the pH of the medium. The effect of pH on removal of arsenate on pure and Cu-HAP was investigated by varying the solution pH from 3.0 to 9.0. Temperature was maintained at 30 °C with contact time 60 min and initial As(V) concentration was 100 μgL^{-1} while adsorbent dosage was maintained 1 gL^{-1}. Fig. 11 shows the effects of pH on adsorption of As(V) on pure and Cu-HAP.

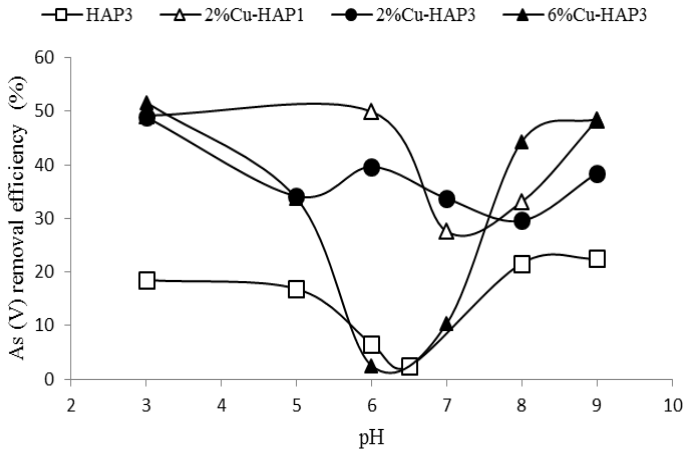

Fig. 11. Effect of pH on removal of As(V) using thermally treated pure and Cu-HAP.

The influence of pH at < 3.0 could not be studied since the adsorbents were not stable at pH < 3.0. Pourbaix diagram for As species [38] indicates that the stable oxidation state, As(V) in aqueous system is a monovalent ($H_2AsO_4^-$) anion in the pH range of 3.0-6.8 or a divalent ($HAsO_4^{2-}$) anion in the pH range of 7.0-11.0. At lower pH, surface of pure and Cu-HAP become highly protonated (< pH_{PZC}) which is favorable for removal of As(V) as the species exists as monovalent anion. For this reason, relatively higher removal efficiency for As(V) is observed at low pH. Moreover, lowest removal efficiency is observed at pH 6.0-7.0, which may be attributed to the pH_{ZPC} values for HAP and Cu-HAP (measured pH_{ZPC} 6.5 and 7.6). A neutral charge condition is developed on surface of the adsorbents at pH 6.0-7.0. With further increase in pH, As(V) removal efficiency increases and reaches a maximum at pH 9.0. Adsorption of As(V) anionic species on negatively charged surface (> pH_{PZC}) of the adsorbents can thus be easily rationalized. The results thus indicate the exchange of arsenate for phosphate in the HAP structure [39].

3.2.3. *Effect of adsorbent dosage*

Fig. 12 shows the effect of dosage variation of pure and Cu-HAP on As(V) removal keeping the other conditions constant. Mass of adsorbent used is an important parameter for the adsorption process since this determines the efficiency of an adsorbent for a given initial concentration of the adsorbate. The equilibrium conditions for studying the adsorption of arsenate are as follows: temperature- 30 °C, contact time- 60 min, pH- 9.0 and initial concentration of arsenate ion- 100 μgL^{-1}.

Fig. 12 shows adsorption of arsenate on HAP3 decreases from 22.48% to 18.69% as adsorbent dosage increases from 1 gL^{-1} to 10 gL^{-1} with a slight increase in the adsorption capacity at HAP3 dosages of 2 and 5 gL^{-1}. Adsorption of As(V) from aqueous media involves exchange of phosphate ion with arsenate ion and concentration of phosphate ion in the solution enhances with increasing exchange of arsenate and phosphate ions. As a consequence, adsorption of arsenate ion on HAP is reduced due to presence of higher phosphate in solution while quantity of HAP increases in the adsorption system [40]. Another reason for reduced adsorption capacity of HAP3 is the lower surface area of the sample which contains less active sites for adsorption. For 6%Cu-HAP3 this capacity enhances from 49% to 60% while this increment is not significant in case of 2%Cu-HAP1 and 2%Cu-HAP3. In cases of Cu-doped HAP, specific surface area of the calcined products is higher in comparison to the pure HAP; therefore higher adsorption efficiency is observed due to the availability of active sites on the materials.

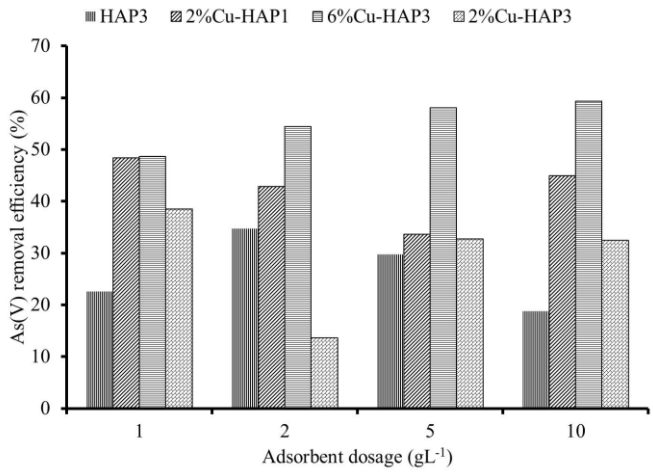

Fig. 12. Effect of adsorbent dosage on removal of As(V) by pure and Cu-HAP.

3.2.4. *Effect of initial concentration of As(V)*

Initial concentrations of arsenate ion were varied in the range of 65-170 μgL^{-1} and keeping other conditions constant. Fig. 13 reveals that adsorption efficiency is higher at lower initial concentration (50 and 90 μgL^{-1}) and gradually decreases with increase in initial

arsenic concentration. The reason for the decrease in As(V) removal efficiency at higher initial concentration may be due to saturation of the active sites of the adsorbent by the As(V) and hence, further increase in As(V) concentration does not bring about an increase in adsorption significantly.

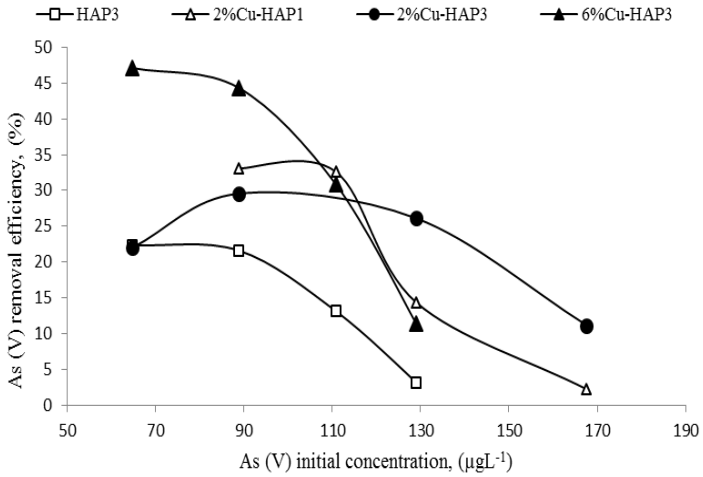

Fig. 13. Effect of initial As(V) concentration on adsorption on pure and Cu-HAP.

Fig. 13 shows that arsenate removal efficiency sharply decreased from 22% to 3% for pure HAP at varying initial As(V) concentration. Nevertheless, Cu-HAP shows (Fig.13) a sharp decrease in As(V) removal efficiency with increase in initial As(V) concentrations as follows: from 47% to 11% for 6%Cu-HAP3, from 22% to 11% for 2%Cu-HAP3 with an initial slight increase to 29.56% and from 33% to 2.21% for 2%Cu-HAP1. Presence of Cu(II) in the adsorbents enhances the adsorption efficiency in comparison to pristine HAP [41].

Table 4 compares the adsorption capacity of a series of adsorbents reported in literature for removal of As(V).

Table 4. Comparison of As(V) adsorption capacity of HAP with other adsorbents.

Type of adsorbent	Adsorbents	Adsorption conditions	Adsorption capacity	Ref.
Other than HAP	Activated alumina	pH 7.6, adsorbent dosage 1-13 g/L	0.18 mg/g	[42]
	Synthetic zeolite H-MFI-24	pH 6.5, adsorbent dosage 2 g/L	35.8 mg/g	[43]
	Modified zeoliteY	pH 6	1.34 mg/g	[44]
	Granular ferric hydroxide (GFH)	pH 6.5, adsorbent dosage 0.25 g/L	1.1 mg/g	[45]
	Iron oxide coated sand	pH 7.5, adsorbent dosage 20 g/L	0.029 mg/g	[45]
	Iron oxide uncoated sand	pH 7.5, adsorbent dosage 20 g/L	0.006 mg/g	[45]

	Magnetite nanoparticle	pH 6, adsorbent dosage 0.4 g/L	8.8 mg/g	[46]
	Granular activated carbon (GAC)	pH 4.7	0.038 mg/g	[47]
	Goethite	pH 6-8, adsorbent dosage 1.6 g/L	4.0 mg/g	[48]
	HAP from fish scale	pH 4, thermally treated at high temperature	0.026 mg/g	[49]
	HAP from bone char	pH 10, thermally treated at high temperature	1.43 mg/g	[50]
	HAP	pH 8, adsorbent dosage 0.3 g/L, hydrothermal process	0.68-9.36%	[51]
	Cu doped HAP	pH 9, adsorbent dosage 0.3 g/L, hydrothermal process	5.75-42%	[52]
HAP	HAP	pH 5-8, commercially available	36%	[53]
	Cellulose carbonate hydroxyapatite nanocomposite	pH 2-10, adsorbent dosage 2 g/L, Microwave-assisted method	3.1 mg/g	[54]
	HAP3	pH 9, adsorbent dosage 1 g/L, Wet chemical method	28.62% or 0.04 mg/g	Present work
	2%Cu-HAP1	pH 9, adsorbent dosage 1 g/L, Wet chemical method	48.33% or 0.06 mg/g	Present work
	6%Cu-HAP3	pH 9, adsorbent dosage 1 g/L, Wet chemical method	48.62% or 0.07 mg/g	Present work

Due to the difference in experimental protocol and synthesis route, an accurate comparison of the removal efficiency is not possible. However, the comparative adsorption capacity has provided the efficiency of Cu-HAP used in this work. As(V) removal efficiency of pure and Cu-HAP has been compared with other adsorbents. 6%Cu-HAP3 showed maximum adsorption capacity of 48.62 % equivalent to 0.07 mg/g, which is superior to some commercial adsorbents along with other HAP-based adsorbents. Few adsorbents like synthetic zeolite H-MFI-24, magnetite nanoparticle, cellulose carbonate hydroxyapatite nanocomposite demonstrated better adsorption capacity. Nevertheless the precursor (eggshells) used for synthesis of pure and Cu-HAP show the promises of the adsorbent since it may contribute in waste management system. By optimization of the synthesis method and also Cu-content of HAP, potential adsorbents could be prepared to remove As(V) that can contribute for sustainable development.

3.3. Adsorption isotherms

The adsorption isotherm provides information on the capacity of the adsorbent or the amount required for removing a unit mass of pollutant under the operating conditions. In this study, Langmuir, Freundlich, and Temkin adsorption isotherms have been adopted to describe the uptake of As(V) on pure and Cu-HAP.

Linear forms of Langmuir, Freundlich, and Temkin isotherm model can be expressed as Eq. (1), (2) and (3) respectively,

$$\frac{C_e}{q_e} = \frac{1}{k_L q_m} + \frac{C_e}{q_m} \quad (1)$$

$$\log q_e = \log K_F + (1/n)\ \log C_e \quad (2)$$

$$q_e = B_1 \ln K_T + B_1 \ln C_e \quad (3)$$

Where q_e is the adsorption capacity at equilibrium (μgg^{-1}), q_{max} is the theoretical maximum adsorption capacity of the adsorbent (μgg^{-1}), K_L is the Langmuir constant (L μg^{-1}) and C_e is the equilibrium As(V) concentration in the solution (μgL^{-1}). q_e is the amount adsorbed per unit mass of adsorbent (μgg^{-1}), C_e is the equilibrium adsorbate concentration in solution (μgL^{-1}), K_F and '*n*' are Freundlich constants related to the adsorption capacity and adsorption intensity respectively. $B_1 = RT/b$, T is temperature in K, R is universal gas constant (8.314 Jmol^{-1}k^{-1}), K_T is the equilibrium binding constant (Lmg^{-1}) and B_1 is related to the heat of adsorption. The magnitude of K_F and n shows easy separation of heavy metal ion from wastewater and high adsorption capacity. If n lies between 1 and 10, this indicates a favorable adsorption process. Results of Langmuir (Fig. 14a), Freundlich (Fig. 14b) and Temkin (Fig. 14c) isotherms are described in Table 4.

Table 5. Parameters of adsorption isotherms.

Sample code	Langmuir adsorption isotherm			Freundlich adsorption isotherm			Temkin isotherm		
	q_m μgg^{-1}	Langmuir constant, K_L, L μg^{-1} (×10^{-2})	R^2	Freundlich constant, K_F, (μg/g) (L/ μg)$^{1/n}$	Freundlich constant, n	R^2	$B_1 = RT/b$	K_T (Lμg^{-1}) (×10^{-3})	R^2
HAP3	2.475	-1.75	0.9730	18.03	-0.5827	0.8871	-14.69	6.00	0.7385
2%Cu-HAP1	1.180	-1.48	0.9084	591.43	-0.4054	0.9674	-20.14	5.93	0.9557
2%Cu-HAP3	7.463	-3.48	0.9974	85.55	-2.2416	0.9879	- 5.95	1.51	0.9234
6%Cu-HAP3	4.810	-2.66	0.9994	3932.78	-0.7457	0.9414	-18.68	6.28	0.8432

The correlation coefficients (R^2) (Table 4) for all the adsorbents are higher than 0.9 and Langmuir constants for pure and Cu-HAP were negative to indicate that the adsorption behavior for As(V) removal system do not follow the assumption on which the Langmuir model is based on. The negative n (Table 4) for As(V) adsorption indicates unfavorable adsorption. The correlation coefficient (R^2) values for the selected adsorbents are lower for Temkin isotherm model considering the R^2 values of Langmuir and Freundlich models. Moreover, values of B_1 (heat of adsorption) are negative for pure and Cu-HAP samples which indicates that this model also does not describe the adsorption process well.

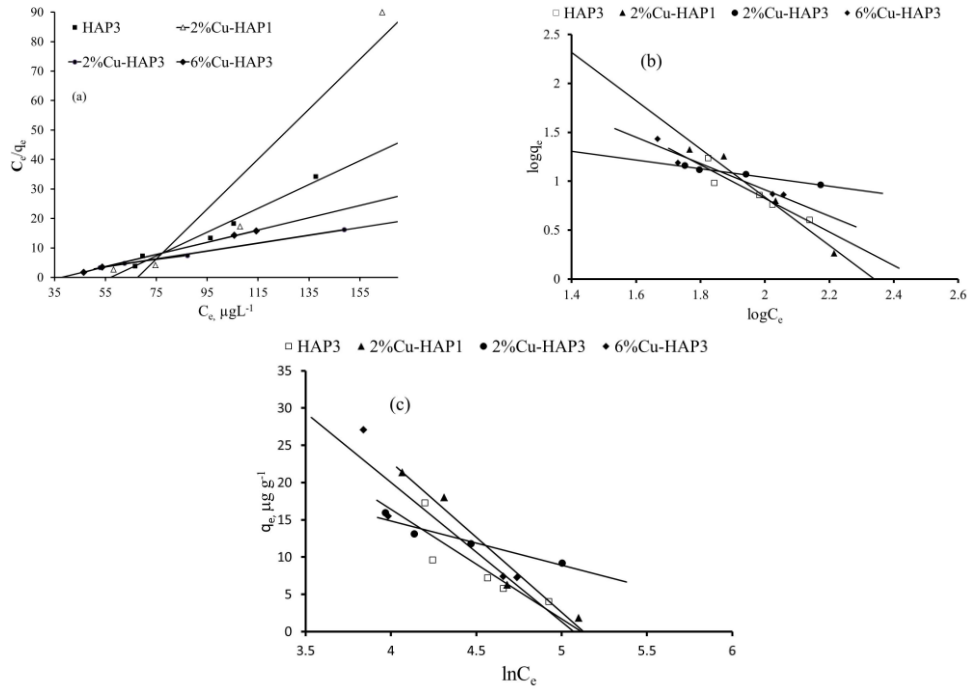

Fig. 14. Adsorption isotherms of (a) Langmuir, (b) Freundlich, and (c) Temkin models for As(V) adsorption on HAP samples.

4. Conclusions

Eggshells are excellent, cost-effective, environment friendly, and sustainable calcium precursors of HAP. Pure and Cu-HAP can be successfully synthesized from eggshells by wet chemical precipitation method. Upon calcination at different temperatures in the range of 110-600 °C they can be employed as adsorbents to remove As(V) from aqueous system. Incorporation of Cu(II) in HAP and thermal treatment at lower temperature facilitates to generate amorphous products with increased specific surface area of the adsorbents. Adsorption studies revealed that equilibrium is established in 60 min at pH 9 with initial As(V) concentration 100 $\mu g^{-1}L^{-1}$ at 30 °C. As(V) removal efficiency of HAP increased from 22% to 48% as a result of Cu(II) incorporation. Adsorption data fit well to the Langmuir, Freundlich, and Temkin isotherm models. However, negative values for the calculated parameters implies the inadequacy of the isotherm models to explain the adsorption process.

Acknowledgment

The authors acknowledge financial support from Higher Education Quality Enhancement Project under the Sub-project, CPSF-231 from Bangladesh University Grants Commission

financed by World Bank and the Ministry of Education, Bangladesh. SAJ also acknowledges the Ministry of Science and Technology, Bangladesh, for 'Bangabandhu Fellowship'.

References

1. D. V. Halem, S. Bakker, G. Amy, and J. V. Dijk, Drinking Water Eng. Sci. **2**, 29 (2009).
2. T. Budinova, D. Savova, B. Tsyntsarski, C. O. Ania, B. Cabal, J. B. Parra, and N. Petrov, Appl. Surf. Sci. **255**, 4650 (2009). https://doi.org/10.1016/j.apsusc.2008.12.013
3. WHO. Arsenic in Drinking Water; Organisation, W. H., Ed.; WHO (Geneva, Switzerland, 2011).
4. R. Singh, S. Singh, P. Parihar, V. Singh, and S. Prasad, Ecotoxicol. Environ. Saf. **112**, 247 (2015). https://doi.org/10.1016/j.ecoenv.2014.10.009
5. Guidelines for Canadian Drinking Water Quality: Guideline Technical Document, by Federal-Provincial-Territorial Committee on Drinking Water of the Federal-Provincial-Territorial Committee on Health and the Environment Health (Canada Ottawa, Ontario, 2006).
6. K. F. Akter, PhD Thesis, University of South Australia Centre for Environmental Risk Assessment and Remediation Mawson Lakes Campus Mawson Lakes, SA 5095 Australia (2006).
7. Y. Chen, F. Parvez, M. Gamble, T. Islam, A. Ahmed, M. Argos, and H. Ahsan, Toxicol. Appl. Pharmacol. **239**, 184 (2009). https://doi.org/10.1016/j.taap.2009.01.010
8. R. Ratnaike, Postgrad. Med. J. **79**, 391 (2003). https://doi.org/10.1136/pmj.79.933.391
9. A. Anjum, P. Lokeswari, M. Kaur, and M. Datta, J. Chromatogr. B, **1**, 25 (2011).
10. T. Singh and K. Pant, Sep. Purif. Technol. **36**, 139 (2004). https://doi.org/10.1016/S1383-5866(03)00209-0
11. D. Mohan and C. U. Pittman, J. Hazard. Mater. **142**, 1 (2007). https://doi.org/10.1016/j.jhazmat.2007.01.006
12. M. Jang, W. Chen, and F. Cannon, Environ. Sci. Technol. **42**, 3369 (2008). https://doi.org/10.1021/es702318f
13. N. R. Nicomel, K. Leus, K. Folens, P. V. D. Voort, and G. D. Laing, Int. J. Environ. Res. Public Health. **13**, 62 (2016). https://doi.org/10.3390/ijerph13010062
14. B. Razzouki, S. E. L. Hajjaji, K. Azzaoui, A. Errich, A. Lamhamdi, M. Berrabah, and L. L. Elansari, J. Mater. Environ. Sci. **6,** 144 (2015).
15. K. Sasaki, H. Nakano, W. Wilopo, Y. Miura, and T. Hirajima, Colloids Surf. A Physicochem. Eng. Asp. **347**, 8, (2009). https://doi.org/10.1016/j.colsurfa.2008.10.033
16. S. A. Jahan, M. Y. A. Mollah, S. Ahmed, and M. A. B. H. Susan, Material Today Proceedings **4**, 5497 (2017). https://doi.org/10.1016/j.matpr.2017.06.005
17. R. Robins – *Proc. Impurity Controland Disposal. CIM Annual Meet.* (Vancouver, Canada, 1985) pp.1/1-1/26
18. W. Anderson, D. Kozak, V. A. Coleman, A. K. Jämting, and M. Trau, J. Colloid. Interf. Sci. **405**, 322 (2013). https://doi.org/10.1016/j.jcis.2013.02.030
19. S. W. Kenneth, R. Sing, and T. Williams, Adsorpt. Sci. Technol. **22**, 773 (2004). https://doi.org/10.1260/0263617053499032
20. S. Brunauer, P. H. Emmett, and E. Teller, J. Am. Chem. Soc. **60**, 309 (1938). https://doi.org/10.1021/ja01269a023
21. E. P. Barrett, L. G. Joyner, and P. P. Halenda, J. Am. Chem. Soc. **73**, 373 (1951). https://doi.org/10.1021/ja01145a126
22. M. H. Ehrampoush, G. Ghanizadeh and M. T. Ghaneian, Iran. J. Environ. Health. Sci. Eng. **8**, 101 (2011).
23. S. Ahmed and M. Ahsan, Bang. J. Sci. Ind. Res. **43**, 497 (2008).
24. G. Liu, J. W. Talley, C. Na, S. Larson and L. G. Wolfe, Environ. Sci. Technol. **44**, 1366 (2010). https://doi.org/10.1021/es1003507

25. R. S. Pillai and V. M. Sglavo, Ceram. Int. **41**, 2512 (2015). https://doi.org/10.1016/j.ceramint.2014.10.073
26. A. Rezakhani and M. M. K. Motlagh, Int. J. Phy. Sci. **7,** 2768 (2012).
27. S. Kannan, J. M. Ventura, and J. M. F. Ferreira, Ceram. Int. **33**, 637 (2007). https://doi.org/10.1016/j.ceramint.2006.05.016
28. L. W. Schroeder and M. J. Mathew, J. Solid State Chem. **26**, 383 (1978). https://doi.org/10.1016/0022-4596(78)90173-1
29. A. Yasukawa, S. Ouchi, K. Kandori, and T. Ishikawa, J. Mater. Chem. **6**, 1401 (1996). https://doi.org/10.1039/JM9960601401
30. J. V. Rau, S. N. Cesaro, D. Ferro, S. M. Barinov, and I. V. Fadeeva, J. Biomed. Mater. Res. Part B: Appl. Biomater. **2**, 441 (2004). https://doi.org/10.1002/jbm.b.30111
31. D. Luna-Zaragoza, E. T. Romero-Guzman, and L. R. Reyes-Gutierrez, J. Miner. Mater. Charac. Eng. **8**, 591 (2009). https://doi.org/10.4236/jmmce.2009.88052
32. C. W. Chen, C. S. Oakes, K. Byrappa, R. E. Riman, K. Brown, K. S. TenHuisen, and V. F. Janas, J. Mater. Chem. **14**, 2425 (2004). https://doi.org/10.1039/B401790K
33. P. Regnier, A. C. Lasaga, R. A. Berner, O. H. Han, and K. W. Zilm, Am. Miner. **79**, 809 (1994).
34. A. ´Sl´osarczyk, Z. Paszkiewicz, and C. Paluszkiewicz, J. Mol. Struct. **744**, 657 (2005).
35. T. Matthias, Chem. Ing. Tech. **82**, 1059 (2010). https://doi.org/10.1002/cite.201000064
36. N. Kannan and K. Karrupasamy, Ind. J. Environ. Protect. **18**, 683 (1998).
37. U. C. Ghosh and S. Goswami, water SA. **31**, 597 (2005).
38. P. L. Smedley and D. G. Kinniburgh, Appl. Geochem. **17**, 517 (2002). https://doi.org/10.1016/S0883-2927(02)00018-5
39. P. Mitchell and J. Gen, Microbiol. **11**, 73 (1954).
40. A. Violante, M. Pigna and R. Ragusa - *17th WCSS* (Thailand, 2002).
41. V. Lenoble, C. Laclautre, V. Deluchat and B. Bollinger, J. Hazard. Mater. B **123**, 262 (2005). https://doi.org/10.1016/j.jhazmat.2005.04.005
42. T. Singh and K. Pant, Sep. Purif. Technol. **36**, 139 (2004). https://doi.org/10.1016/S1383-5866(03)00209-0
43. P. Chutia, S. Kato, T. Kojima, and S. Satokawa, J. Hazard. Mater. **162**, 440 (2009). https://doi.org/10.1016/j.jhazmat.2008.05.061
44. A. M. Yusof and N. A. Malek, J. Hazard. Mater. **162**, 1019 (2009). https://doi.org/10.1016/j.jhazmat.2008.05.134
45. V. Gupta, V. Saini, and N. Jain, J. Colloid Interface Sci. **288**, 55 (2005). https://doi.org/10.1016/j.jcis.2005.02.054
46. P. Roy, M. Choudhury, and M. Ali, Int. J. Chem. Environ. Eng. **4**, 55 (2013).
47. Z. Gu, J. Fang, B. Deng, Environ. Sci. Technol. **39**, 3833 (2005). https://doi.org/10.1021/es048179r
48. V. Lenoble, O. Bouras, V. Deluchat, B. Serpaud, and J. Bollinger, J. Colloid Interface Sci. **225**, 52 (2002). https://doi.org/10.1006/jcis.2002.8646
49. M. S. Rahaman, A. Basu, and M. R. Islam, Bioresour. Technol. **99**, 2815(2008). https://doi.org/10.1016/j.biortech.2007.06.038
50. Y. N. Chen, L. Y. Chai, and Y. D. Shu, J. Hazard. Mater. **160**, 168 (2008). https://doi.org/10.1016/j.jhazmat.2008.02.120
51. G. Liu, J. W. Talley, C. Na, S. Larson, and L. G. Wolfe, Environ. Sci. Technol. **44,** 1366 (2010). https://doi.org/10.1021/es1003507
52. M. Mirhosseini, E. Biazar, and K. Saeb, Curr. World Environ. **9**, 331 (2014). https://doi.org/10.12944/CWE.9.2.13
53. W. E. Alson - *Denver Annual Meeting* (2002).
54. P. C. Mishra and R. M. Islam Patel, J. Hazard. Mater. **189**, 755 (2011). https://doi.org/10.1016/j.jhazmat.2011.03.051